

Fe-doped ZnS film fabricated by electron beam evaporation and its application as saturable absorber for Er:ZBLAN fiber laser

Jiu-Lin Yang(杨久林), Guo-Ying Feng(冯国英), Du-Xin Qing(卿杜鑫), Ya-Jie Wu(吴雅婕), Yun Luo(罗韵), and Jian-Jun Wang(王建军)

Citation: Chin. Phys. B, 2021, 30 (**7**): 074207. DOI: 10.1088/1674-1056/abf343
Journal homepage: http://cpb.iphy.ac.cn; http://iopscience.iop.org/cpb

What follows is a list of articles you may be interested in

Influences of annealing temperature on properties of Fe^{2+}: ZnSe thin films deposited by electron beam evaporation and their applications to *Q*-switched fiber laser

Du-Xin Qing(卿杜鑫), Shu-Tong Wang(王树同), Shou-Gui Ning(宁守贵), Wei Zhang(张伟), Xiao-Xu Chen(陈晓旭), Hong Zhang(张弘), Guo-Ying Feng(冯国英), Shou-Huan Zhou(周寿桓)
Chin. Phys. B, 2020, 29 (**5**): 054208. DOI: 10.1088/1674-1056/ab81f2

Zinc-oxide nanoparticle-based saturable absorber deposited by simple evaporation technique for Q-switched fiber laser

Syarifah Aloyah Syed Husin, Farah Diana Muhammad, Che Azurahanim Che Abdullah, Siti Huzaimah Ribut, Mohd Zamani Zulkifli, Mohd Adzir Mahdi
Chin. Phys. B, 2019, 28 (**8**): 084207. DOI: 10.1088/1674-1056/28/8/084207

Effects of annealing time on the structure, morphology and stress of gold-chromium bilayer film

Hong Zhang(张洪), Yun-Xia Jin(晋云霞), Hu Wang(王虎), Fang-Yu Kong(孔钒宇), Hao-Peng Huang(黄昊鹏), Yun Cui(崔云)
Chin. Phys. B, 2016, 25 (**10**): 104205. DOI: 10.1088/1674-1056/25/10/104205

High refractive index sensitivity sensing in gold nanoslit arrays

Yuan Jun, Kan Qiang, Geng Zhao-Xin, Xie Yi-Yang, Wang Chun-Xia, Chen Hong-Da
Chin. Phys. B, 2014, 23 (**8**): 084201. DOI: 10.1088/1674-1056/23/8/084201

Wide-angle and broadband graded-refractive-index antireflection coatings

Zhang Jun-Chao, Xiong Li-Min, Fang Ming, He Hong-Bo
Chin. Phys. B, 2013, 22 (**4**): 044201. DOI: 10.1088/1674-1056/22/4/044201

Fe-doped ZnS film fabricated by electron beam evaporation and its application as saturable absorber for Er:ZBLAN fiber laser*

Jiu-Lin Yang(杨久林)[1], Guo-Ying Feng(冯国英)[1,†], Du-Xin Qing(卿杜鑫)[1], Ya-Jie Wu(吴雅婕)[1], Yun Luo(罗韵)[2], and Jian-Jun Wang(王建军)[2]

[1] *Institute of Laser & Micro/Nano Engineering, College of Electronics and Information Engineering, Sichuan University, Chengdu* 610064, *China*
[2] *Research Center of Laser Fusion, China Academy of Engineering Physics, Mianyang* 621900, *China*

(Received 2 January 2021; revised manuscript received 26 March 2021; accepted manuscript online 30 March 2021)

High-quality Fe-doped ZnS films have been fabricated by electron beam evaporation. After the doping, the fabricated films still maintain the preferential crystalline orientation and phase purity of the host ZnS. According to the observation of surface morphology, the root mean-square roughness of the samples increases slightly with the increase of doping content. All of the prepared samples are in cubic zinc blende structure of ZnS. Transmission spectrum confirms a more obvious dip near 3 μm with higher dopant concentration and it can be attributed to the typical $^5E \rightarrow {}^5T_2$ transition of Fe^{2+}. Fe-doped ZnS film is also successfully used for *Q*-switched Er:ZBLAN fiber laser.

Keywords: Fe-doped ZnS film, electron beam evaporation, *Q*-switching, Er:ZBLAN

PACS: 42.60.Gd, 42.70.Hj **DOI:** 10.1088/1674-1056/abf343

1. Introduction

The laser radiation in the mid-infrared band has extensive application in the fields of molecular spectroscopy, environmental remote sensing, space communication, industrial processing, and medical treatment.[1–4] Transition metal substitution in II–VI semiconductors has aroused widespread interest as laser materials for the mid infrared laser, both as gain media and saturable absorbers. II–VI sulfide crystal matrix materials mainly include binary sulfides (such as ZnS, ZnSe, CdSe, CdS, and ZnTe) and ternary sulfides (such as CdMnTe, CdZnTe, and ZnSSe).[5,6] Both ZnSe and ZnS have high transmittance as infrared laser materials. Compared with ZnSe, ZnS matrix materials possess a higher damage threshold, lower cost, better thermal lens resistance and thermal damage resistance.[7] In addition, ZnS crystal exhibits higher solidity, lower dependence on refractive index and third-order nonlinearity upon temperature.[8] These desirable properties make ZnS a promising candidate for mid infrared laser systems.

Fe^{2+} is one of the most significant dopants for the mid-infrared lasers based on transition metal ions.[9,10] Fe-doped ZnS material has been paid an increasing attention as gain media and saturable absorber.[10,11] In 2011, Kozlovsky *et al.* demonstrated a laser with tunable wavelength within the range of 3.49–4.65 μm for the first time, by using Fe^{2+}:ZnS crystal as gain material.[12] Subsequently, plenty of work on the investigations of Fe doped ZnS has been published.[13–18] Due to the electron-vibrational transitions $^5E \rightarrow {}^5T_2$ of Fe^{2+} (electron configuration $3d^6$) substituting the Zn^{2+} cations in the tetragonal position,[19] it also provides a wide absorption band centered around 3 μm and can be applied to passively *Q*-switched lasers.[20] Using Fe^{2+}:ZnS saturable absorber, Boris Denke *et al.* reported short pulse generation of a 2.3 μm Tm-doped tellurite glass laser.[21] Fe-doped ZnS crystal for passive *Q*-switching of 2.8 μm Er-doped laser has been demonstrated.[22] These applications were all based on the Fe-doped ZnS bulk crystal. The doping of Fe into ZnS bulk crystal can be performed during post-growth or crystallization process for single crystal and polycrystalline samples. For the former process, a thin film of the metal to be doped is deposited on the surface of bulk ZnS. However, the following thermal diffusion always inevitably brings about a rapid variety of concentration profile near the surface.[23,24]

Thin film devices can often offer compactness and the advantage that both dopant profile and deposition rate can be controlled during deposition process. Recent work on fabrication of Fe-doped ZnS film suggests a new route to the fabrication of saturable absorber for passive *Q*-switching.[10,25] The latest report on physical fabrication method of Fe:ZnS film is MBE-grown method,[25] which requires an ultra-high vacuum environment and related equipment with better performance. Otherwise, the quality of the deposited film cannot be well guaranteed. Here, we report Fe-doped ZnS films fabricated by electron beam evaporation (EB) and it can avoid the aforementioned disadvantage of the MBE-grown method and reduce the chance of contamination. We also investigate the surface morphology, the structural and optical absorption properties of the prepared films. Furthermore, the sample is also applied as saturable absorber for *Q*-switched Er:ZBLAN fiber laser.

*Project supported by the National Natural Science Foundation of China (Grant No. U1730141).
†Corresponding author. E-mail: guoing_feng@scu.edu.cn
© 2021 Chinese Physical Society and IOP Publishing Ltd

2. Experimental details

Fe-doped ZnS films with different concentrations of Fe were prepared by electron beam evaporation. The substrates were double-side polished sapphire, gold-plated mirror, and silicon wafer. Polycrystalline ZnS granule (high purity, 99.99%) and Fe powder (high purity, 99.99%) were chosen as the targets. The samples were deposited on the substrates in an electron beam evaporation chamber and the substrate temperature was kept at 250 °C. The films were prepared at the pressure between 3.5×10^{-3} Pa and 2×10^{-4} Pa during the process of deposition. Before deposition, the substrates were successively purged in ultrasound baths of acetone, ethanol, deionized water, ethanol and then blown dry with nitrogen. The deposition rate for Fe and ZnS was 0.1–0.2 Å/s and 1.0–1.4 Å/s, respectively. The substrates were held in a rotating sample holder and rotated with a rate of 20 rpm. SQC-310 rate controller (INFICON) and a quartz crystal monitor were used to monitor the deposition rate and film thickness. Once the temperature dropped slowly to room temperature, the films were quickly loaded in a furnace to anneal at 400 °C at a pressure below 2×10^{-3} Pa for about 10 hours.

Study of surface morphology and structure was carried out using atomic force microscope (AFM , ASYLUMRESEARCH, MFP-3D-BIO) and x-ray diffraction (XRD). Elemental composition of the films was determined by energy-dispersive x-ray spectroscopy (EDS) system. Raman spectra were recorded with 532 nm excitation source laser. The spectral transmission information at room temperature was measured with a Fourier transform infrared spectrometer (Bruker, Tensor27) in the wavelength range of 1000 nm to 5000 nm.

3. Results and discussion

3.1. Elemental composition and AFM results

For the prepared films, the doping level of Fe was determined to be 0.34 at%, 0.49 at%, 0.93 at%, and 1.34 at%, respectively. The surface morphology of Fe:ZnS thin films was analyzed using AFM in a scanning area of 5×5 μm^2. Figure 1 shows the 3D topographic AFM images (the vertical height is 80 nm) of the films deposited on sapphire substrate with different concentration. Figure 2 shows a typical EDS pattern. The roughness of the thin films was analyzed according to its root mean-square (RMS) roughness value. The corresponding value of RMS surface roughness was determined to be 8.05 nm, 8.8 nm, 8.94 nm, and 12.18 nm, successively. The RMS of the Fe-doped ZnS thin films increased with the increase of Fe-concentration. Within a certain range of doping concentration, the similar trend has been reported in Refs. [26,27]. This kind of relatively flat surface of the deposited films will not cause too much scattering loss.

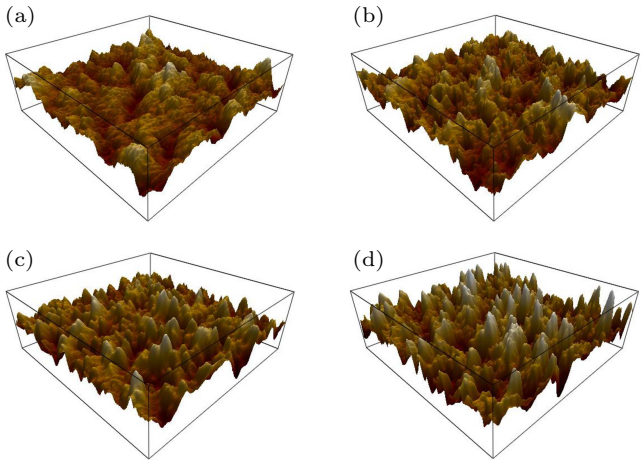


Fig. 1. The 3D AFM image (the vertical height is 80 nm and the scanning area is 5×5 μm^2) of the samples with concentration of (a) 0.34 at%, (b) 0.49 at%, (c) 0.93 at%, and (d) 1.34 at%.

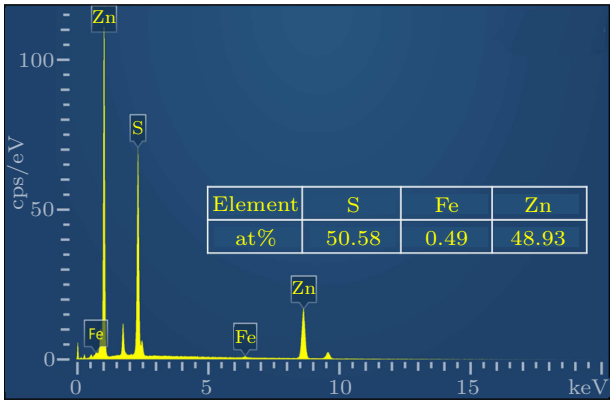


Fig. 2. Typical EDS pattern for Fe:ZnS film of which the Fe-concentration was determined to be 0.49 at%.

3.2. XRD analysis

The crystalline properties of the deposited Fe-doped ZnS films were characterized by grazing incidence XRD with a grazing angle of 1° and 2θ angles of 20°–90°. Figure 3 shows the XRD patterns of Fe:ZnS films with different concentrations of Fe and JCPDS card (PDF#05-0566) for cubic ZnS. It can be seen from the figure that the diffraction peaks of all Fe-doped ZnS films appear around 28.6°, 47.7°, and 56.4°. In comparison with the JCPDS standard card, they correspond to the three crystal planes of {111}, {220} and {311} for ZnS, respectively. It can be found that the diffraction peaks are consistent with cubic zinc blende structure of zinc sulfide for all of the prepared films. As for the sample with a concentration of 1.34 at%, a peak around 40.7° may result from the oxidation products, comparing with JCPDS card (PDF#49-1447 and PDF#13-0311). Based on these results, phase purity and preferential crystalline orientation of the host ZnS films were retained when a certain amount of iron was doped. All samples possess strongly preferred orientation along {111} and obviously weak peak along {220} and {311}, which is different from JCPDS card. It can be accounted for the rearrangement

of atoms and the regrowth occurred in the films. Good crystallinity of these films can be inferred from the small full width at half maximum (FWHM) of narrow peaks.

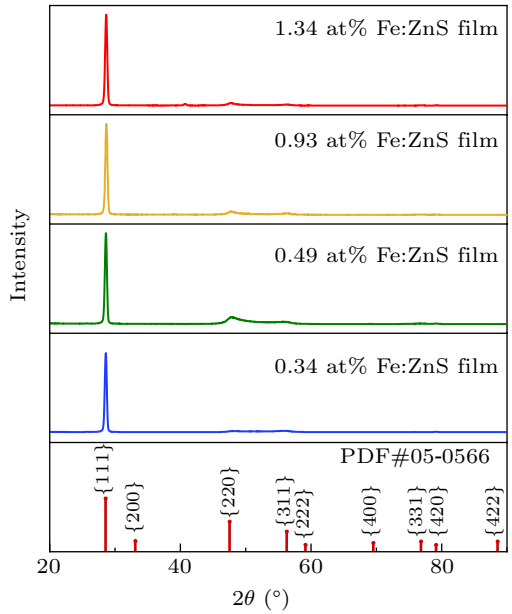


Fig. 3. XRD pattern of Fe^{2+}:ZnS films and cubic ZnS bulk polycrystal.

3.3. Raman analysis

Figure 4 displays the Raman spectra in the range of 100–700 cm^{-1} for the films with different content of iron, the corresponding substrates are sapphire. The Raman peaks around 350 cm^{-1} and 645 cm^{-1} are the characteristic Raman modes of ZnS. Taking into consideration of the results of XRD characterization, the Raman modes can be identified as T_2(LO), 2(TO) for zinc blende ZnS.[28–30] These results indicate that the samples all retain the Raman modes of pure ZnS with the doping of iron. The results also show that the intensity of the 2(TO) mode increases with higher doping concentration.

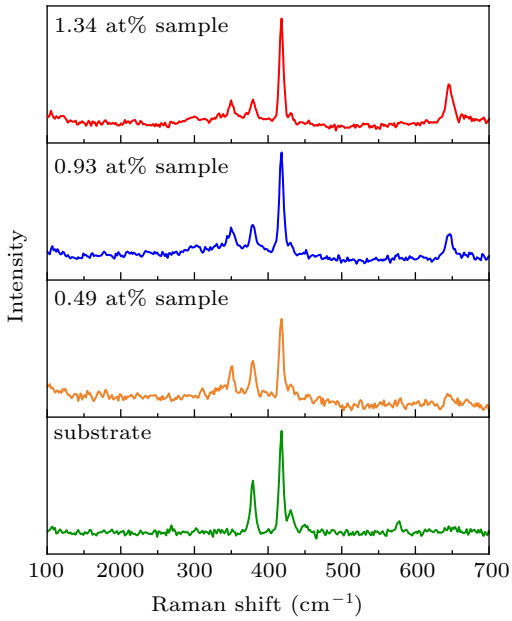


Fig. 4. Raman spectra of Fe:ZnS films with different Fe concentrations.

3.4. Optical transmission

Figure 5(a) shows the optical transmittance recorded in 1000–5000 nm of the prepared Fe-doped ZnS films with different content of iron. By the method of Swanepoel analysis,[31,32] the thickness and absorption coefficients were calculated for the prepared films. According to the interference fringes of the transmission spectrum, the thicknesses (D) of these films can be estimated using the following equation:[31]

$$D = \frac{\lambda_1 \lambda_2}{2(\lambda_1 n_2 - \lambda_2 n_1)}, \tag{1}$$

where λ_1 and λ_2 are the wavelengths at two adjacent maximums (or minimums) of the interference fringes, and the refractive indices of the corresponding wavelengths are respectively to be n_1 and n_2. The estimated value of thicknesses for the samples are both about 2.85 μm. Good homogeneity can be inferred from the interferometric fringe and $^5E \rightarrow {}^5T_2$ transition of Fe^{2+} in ZnS host cause the obvious transmission dip near 3 μm. With the increase of Fe^{2+}-content, more obvious dip of the transmission can be found in the curve and the estimated absorption coefficients for the fabricated samples can be found in Fig. 5(b).

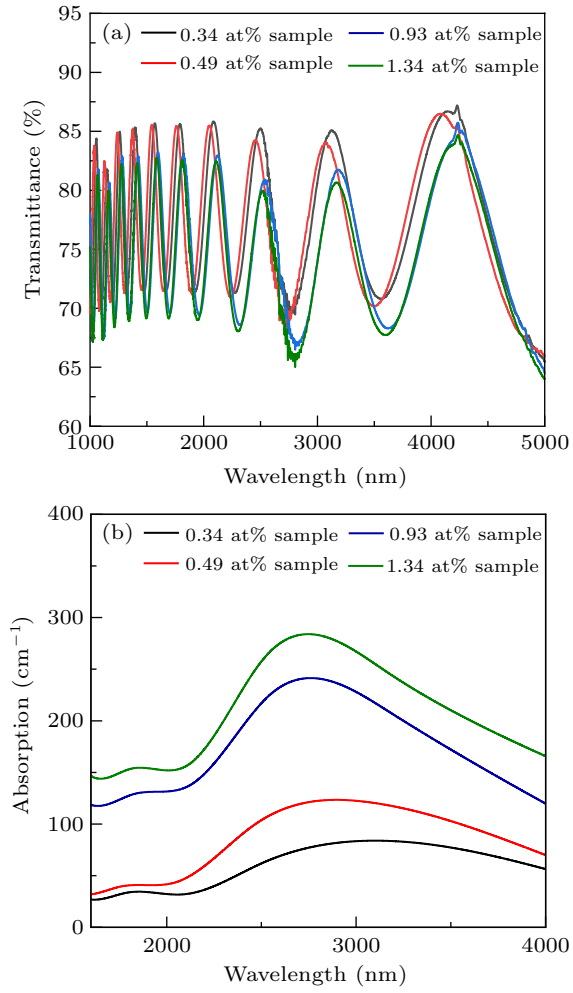


Fig. 5. (a) The transmission for Fe:ZnS film with different Fe concentration; (b) the estimated absorption coefficient of corresponding samples.

3.5. The *Q*-switching for Er:ZBLAN fiber laser

One sample which has about twice thickness of Fe-doped ZnS films with 0.49 at% of Fe was chosen as saturable absorber for the *Q*-switched fiber laser, and they have the same doping ratio. A simple linear cavity as shown in Fig. 6 was constructed to certify the saturable absorption of the Fe-doped ZnS film. The pump source is a commercial 976 nm laser diode. A highly Er^{3+}-doped ZBLAN fiber of which the Er^{3+} doping concentration is 6 mol.% serves as the gain fiber and its length is about 2 m. As for the gain fiber, its core diameter and NA are respectively to be 33 μm and 0.12. The core diameter and NA of the gain fiber's octagonal inner cladding are respectively 330 μm and 0.5. The focus lengths of the two plano-convex CaF_2 lenses are both 35 mm. The input end of the gain fiber was flat-angle cleaved, and the rear end of the gain fiber was cleaved with an angle of 6° to reduce parasitic oscillation. Both end of the gain fiber are mounted in a water-cooled fiber aluminum heat sink. After the gain fiber, two concave reflective mirrors (M1 and M2, high-reflection coating from 2.5 μm to 3.0 μm) of which the radius curvature are 100 mm and 50 mm respectively, are parallel-placed as much as possible to focus the laser beam onto the Fe:ZnS-SAM. Among the two CaF_2 lenses, a dichroic mirror (DM) is mounted at 45°. The DM possesses high reflection (> 99%) at 2.8 μm and a high transmittance (> 98%) at 976 nm.

Figure 7(a) shows the average output power as a function of pump power and the maximum average output power is 441 mW at the maximum pump power. The turning corresponds to the pump power about 5 W may be caused by the influence of thermal effect and slight spatial location change of Fe:ZnS-SAM during test. Figure 7(b) shows that the pulse width decreases from 2.284 μs to 771 ns and the repetition rate increases from 30.73 kHz to 94.24 kHz with the launched pump power from 2.09 W to 9.93 W. Typical pulse trains and the corresponding single pulse waveform from passively *Q*-switched laser for different pump power are presented in Figs. 8(a) and 8(b).

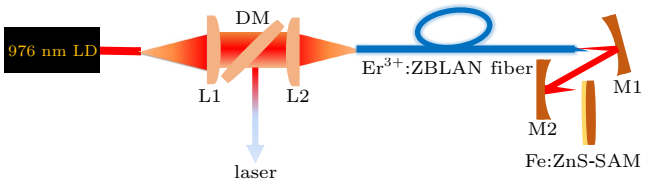


Fig. 6. Experimental setup for *Q*-switched Er:ZBLAN fiber laser.

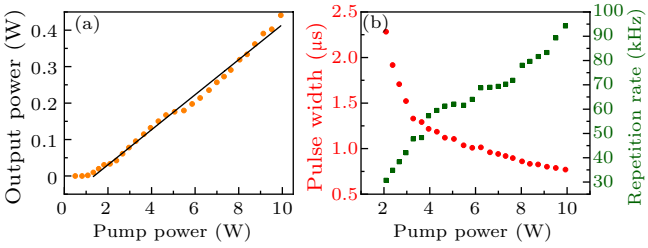


Fig. 7. (a) Average output power as a function of pump power; (b) the pulse width and the repetition rate as a function of pump power.

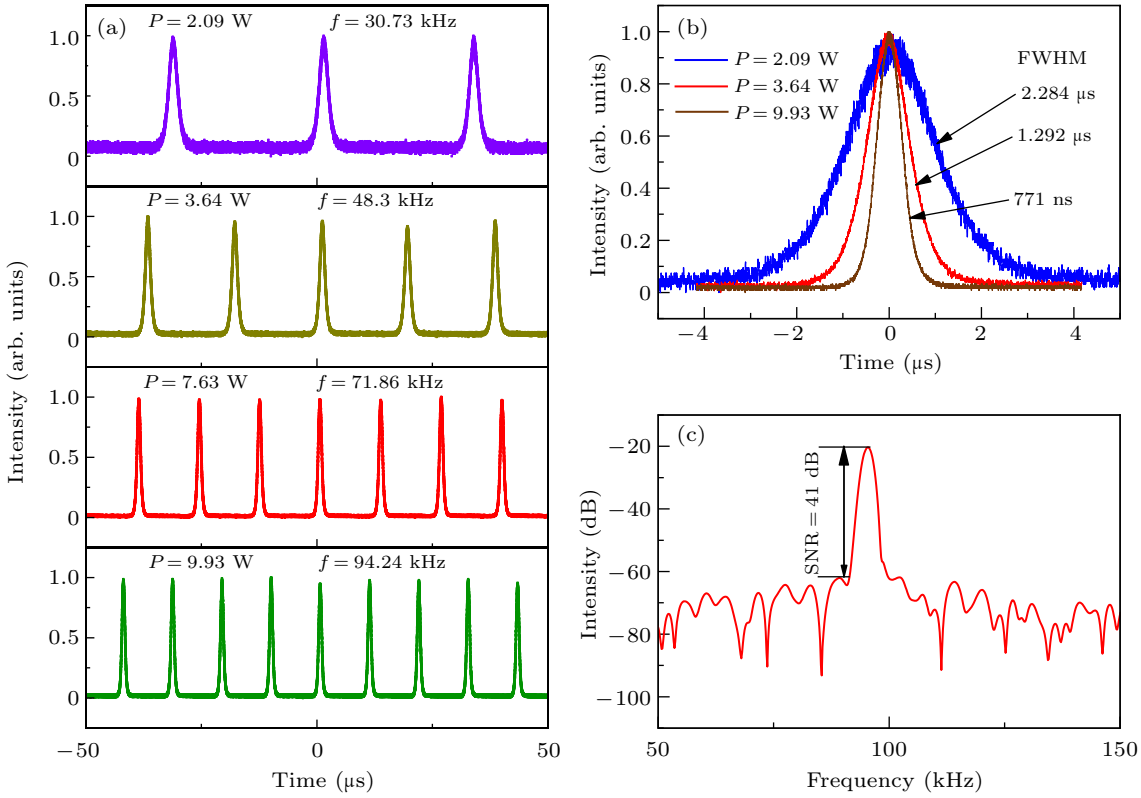


Fig. 8. (a) Typical pulse trains at different pump power; (b) the corresponding single pulse waveform; (c) RF output spectrum at the pump power of 9.93 W.

The maximum pump power is lower than 10 W to avoid catastrophic damage to the fiber end-face. At the maximum pump power of 9.93 W, the radio-frequency spectrum displays a 41 dB signal-to-noise ratio (SNR), as shown in Fig. 8(c), and it demonstrates a stable Q-switching operation. At the pump power of 4.31 W, the output spectrum with a relatively narrow FWHM of 1.6 nm was measured and the center wavelength is $\sim$ 2773 nm, as shown in Fig. 9. Fe-doped ZnSe film had also been successfully used as saturable absorber for Er:ZBLAN fiber laser and the results of optical spectrum were shown in Table 1. Fe:ZnSe and Fe:ZnS are both important saturable absorber for Er-doped laser and the former reports are valuable work. And our work is also useful practice for related applications.

Table 1. Comparison of optical spectrum of the Q-switched Er^{3+}-doped ZBLAN fiber laser by Fe:ZnSe and Fe:ZnS film.

Reference	SA	Wavelength (nm)	FWHM (nm)
[33]	Fe:ZnSe	2779.2 nm	5.2 nm
[34]	Fe:ZnSe NCs film	$\sim$ 2780 nm	3 nm
This work	Fe:ZnS	$\sim$ 2773 nm	1.6 nm

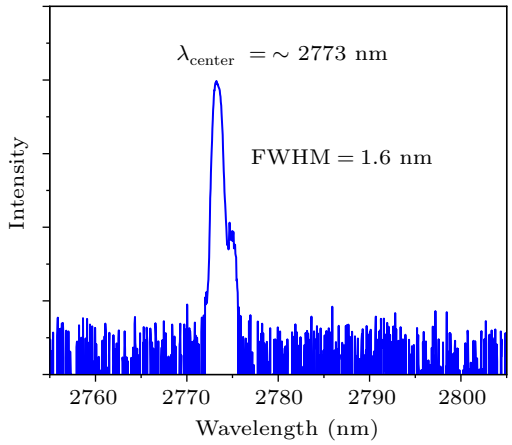


Fig. 9. The laser output spectrum at the pump power of 4.31 W.

4. Conclusion

Fe-doped ZnS films with different concentration of Fe were deposited via using electron beam evaporation. The results of AFM indicate that the value of root mean square roughness for the Fe-doped ZnS films slightly increase with the increasing content of Fe^{2+}. The characterization results of XRD and Raman spectra configure the structure of cubic ZnS. Transmission spectrum shows an obvious dip near 3 μm and it can be attributed to the typical $^5E \rightarrow {}^5T_2$ transition of Fe^{2+} incorporated into ZnS matrix. The prepared film was also applied as saturable absorber for Q-switched Er:ZBLAN fiber laser.

References

[1] Ma J, Qin Z, Xie G, Qian L and Tang D 2019 *Appl. Phys. Rev.* **6** 021317
[2] Xu H, Xu D, Chen S, Ma W and Shi Z 2020 *Remote Sens-Basel* **12** 1512
[3] Fang B, Bodepudi S C, Tian F, Liu X, Chang D, Du S, Lv J, Zhong J, Zhu H, Hu H, Xu Y, Xu Z, Gao W and Gao C 2020 *Nat. Commun.* **11** 6368
[4] Fang Y, Ge Y, Wang C and Zhang H 2020 *Laser Photonics Rev.* **14** 1900098
[5] Fedorov V, Martyshkin D and Mirov S 2018 *Advanced Solid State Lasers* 2018, November 4–8, 2018, Boston, USA, p. AW3A.6
[6] Fedorov V, Martyshkin D, Karki K and Mirov S 2019 *Opt. Express* **27** 13934
[7] Loiko P, Vitkin V, Balabanov S, Dymshits O, Grigorenko K, Polishchuk A, Volokitina A, Mateos X, Serres J M and Gavrishchuk E 2019 *Laser Phys. Lett.* **16** 065801
[8] Sorokina I T 2004 *Opt. Mater.* **26** 395
[9] Evans J W, McDaniel S A, Stites R W, Berry P A, Cook G, Harris T R and Schepler K L 2020 *Solid State Lasers XXIX: Technology and Devices*, February 21, 2020, San Francisco, USA, p. 112590C
[10] Polyakov S M, Karhu E, Zamiri R, Moisset C, Iliopoulos K, Vullum P E, Osterberg U L and Gibson U J 2018 *Opt. Mater. Express* **8** 356
[11] Lu X, Li J, Yang L, Ren J, Sun M, Yang A, Yang Z, Jain R K and Wang P 2020 *Opt. Lett.* **45** 2676
[12] Kozlovsky V I, Korostelin Y V, Landman A I, Mislavskii V V, Podmar'kov Y P, Skasyrsky Y K and Frolov M P 2011 *Quantum Electron.* **41** 1
[13] Fedorov V V, Martyshkin D, Mirov M, Moskalev I, Vasilyev S, Peppers J, Mirov S and Gapontsev V 2013 *CLEO: Applications and Technology* 2013, June 9–14, 2013, San Jose, USA, p. JM4K.2
[14] Frolov M P, Korostelin Y V, Kozlovsky V I and Podmar'kov Y P 2015 *Laser. Phys. Lett.* **12** 055001
[15] Firsov K N, Gavrishchuk E M, Ikonnikov V B, Kazantsev S Y, Kononov I G, Rodin S A, Savin D V and Timofeeva N A 2016 *Laser. Phys. Lett.* **13** 015001
[16] Kozlovsky V, Korostelin Y, Podmar'kov Y, Skasyrsky Y and Frolov M 2016 *J. Phys: Conf. Ser.* **740** 012006
[17] Mirov S B, Moskalev I S, Vasilyev S, Smolski V, Fedorov V V, Martyshkin D, Peppers J, Mirov M, Dergachev A and Gapontsev V 2018 *IEEE J. Sel. Topics Quantum Electron.* **24** 1601829
[18] Gafarov O, Martyshkin D, Fedorov V and Mirov S 2018 *Solid State Lasers XXVII: Technology and Devices*, February 15, 2018, San Francisco, USA, p. 105111R
[19] Kisel V, Shcherbitskii V, Kuleshov N, Postnova L and Levchenko V 2005 *J. Appl. Spectrosc.* **72** 818
[20] Deloach L D, Page R H, Wilke G D, Payne S A and Krupke W F 1996 *IEEE J. Quantum Electron.* **32** 885
[21] Denker B, Dorofeev V, Galagan B, Korostelin Y, Kozlovsky V, Motorin S and Sverchkov S 2018 *Laser Phys. Lett.* **15** 105801
[22] Martinez A, Gallian A, Marine P, Fedorov V, Mirov S and Badikov V 2007 *Advanced Solid-State Photonics 2007*, January 28–31, 2007, Vancouver, Canada, p. TuB24
[23] Myoung N, Fedorov V V, Mirov S B and Wenger L E 2012 *J. Lumin.* **132** 600
[24] Migal E A, Balabanov S S, Savin D V, Ikonnikov V B, Gavrishchuk E M and Potemkin F V 2021 *Opt. Mater.* **111** 110640
[25] Molland N A, Ghadyani Z, Karhu E A, Poggio S, Nematollahi M, Kildemo M, Reenaas T W, BelBruno J J and Gibson U J 2015 *Opt. Mater. Express* **5** 1613
[26] Sreedhar M, Neelakanta Reddy I, Bera P, Shyju T S and Anandan C 2017 *Surf. Interface Anal.* **49** 284
[27] Shobana M and Meher S R 2019 *Thin Solid Films* **683** 97
[28] Nilsen W G 1969 *Phys. Rev.* **182** 838
[29] Brafman O and Mitra S S 1968 *Phys. Rev.* **171** 931
[30] Cheng Y C, Jin C Q, Gao F, Wu X L, Zhong W, Li S H and Chu P K 2009 *J. Appl. Phys.* **106** 123505
[31] Swanepoel R 1983 *J. Phys. E-Sci. Instrum.* **16** 1214
[32] Minkov D and Swanepoel R 1993 *Opt. Eng.* **32** 3333
[33] Zhang T, Feng G, Zhang H, Yang X, Dai S and Zhou S H 2016 *Laser. Phys. Lett.* **13** 075102
[34] Ning S G, Feng G Y, Zhang H, Zhang W, Dai S Y, Xiao Y, Li W, Chen X X and Zhou S H 2018 *Opt. Mater. Express* **8** 865